RESEARCH PAPER

Effect of Silica Content on Support-Iridium Active Phase Interactions on the Nanocatalyst Activity

Zahra Amirsardari *, Akram Dourani, Fatemeh Hasanpour, Mohamad Ali Amirifar, Nooredin Ghadiri Massoom

Department of Nanotechnology, Space Transportation Research Institute, Iranian space research center, Tehran, Iran

ARTICLE INFO

ABSTRACT

To discuss the potential role of the support for iridium catalyst, we have proceeded to prepare a series of supported catalysts with the same active phase content, but different silica content, to elucidate the changes in surface structure and the reaction process of hydrous hydrazine decomposition on catalyst. The obtained iridium catalysts contained 20 wt% of nanoparticles dispersed on spherical mesoporous alumina and aluminosilicate supports for hydrogen generation from hydrous hydrazine. Iridium nanoparticles with different morphologies and diameters could be produced over the catalyst supports depending on its nature. The iridium catalysts were characterized by some techniques such as XRD, FESEM, BET, TGA, H_2-TPR, and mechanical properties. The type of catalyst support played an important role in the effectiveness of the catalyst particles, leading to different activities for hydrazine monohydrate decomposition. Under the given test conditions, the performance of the catalyst was better when using alumina granular as the catalyst support than when using aluminosilicate granular. Since the aluminosilicate support was less reactive than the alumina, hydrogen selectivity was relatively small; consequently, the reaction rate was lower when using the aluminosilicate support than when using the alumina support.

INTRODUCTION

The synthesis process and applications of nanocatalysts are an integral part of nanotechnology and catalysis science that reported in pervious researches [1–4]. The catalyst carriers play an important role in determining the rate of the catalytic reaction although it does not directly participate in the reaction [5–7]. In general, a suitable support with high specific surface area should have various superior properties such as high physical/chemical stability and high thermal/mechanical strength [8]. There is some controversy in the literature about the role and the influence of the support on the activity of active phase nanoparticles [9]. Among the different types of supports used in heterogeneous catalysis, alumina and aluminosilicate are the good carries due to their superior properties [10,11]. Ultra high temperature ceramics and their composites can be used as a supports with excellent heat resistance in the system, but the cost will be very high [12–15]. The most important and cheapest support is gamma-alumina ($γ-Al_2O_3$) with uniform pore size distribution. This kind of support is object-specific in high porosity and surface area to volume ratio, and also the chemical, thermal and mechanical stability [16,17]. The base line support was the granular activated alumina used in standard

* Corresponding Author Email: Z.amirsardari@isrc.ac.ir

Shell-catalyst manufacture. But granular alumina containing approximately 6% SiO_2 was produced by Esso Research and Engineering Company [18]. MCM-41 as acidic support with low to moderate Brønsted acidity is suitable material for catalyst preparation. The surface of silica support, unlike alumina, contains hydroxyl groups, which exhibits no Brønsted acidity, but its acidity can be tuned by incorporating Al into the silica framework, thus generating weak to moderately acidic sites. It is possible to adjust the acid content of aluminosilicate by changing the Si/Al ratio [19].

Unfortunately, there are no effort data associated with the use and different comparison of silica–alumina as a catalyst carrier for the hydrazine decomposition. Hydrazine (N_2H_4) is a fuel with high energy content and hydrogen-rich product [20]. N_2H_4 is a very active compound, and can be decomposed to N_2 and H_2 on catalysts at room temperature [21]. Various catalyst supports have been used for hydrazine decomposition [14–16]. Among the metal centers active as catalysts for the N_2H_4 decomposition reaction, iridium (Ir) has been preferred for developing new catalytic systems because of previous screening tests performed by the authors on the metal supported that indicated iridium as the most promising catalyst for hydrazine decomposition [25–27]. 20–40 wt% iridium active phase is used as catalyst for N_2H_4 decomposition. Iridium nanoparticles exhibit low H_2 selectivity [28]. Therefore, the development of efficient and selective catalysts with special supports for gas generation with high temperature production from hydrazine is critical importance in some systems.

In the present paper, some catalysts with different silica–alumina composition were employed to study the characteristics of N_2H_4 as well as its decomposition gases and intermediate products on Ir based catalysts with same active phase contents (20 wt%) and different supports (alumina with different silica content) to elucidate the changes in surface structure and the hydrazine decomposition reaction. We found a drastic change in iridium dispersion by changing the support type. Because varieties of iridium catalysts with different Ir dispersions could be prepared by controlling the silica content alone, dispersion effects on the catalytic activity during decomposition were readily identified using catalysts prepared through the same procedure, eliminating the effects of preparation variables.

MATERIALS AND METHODS
Catalyst preparation by porous impregnation

Hydrazine monohydrate ($N_2H_4 \cdot H_2O$, Merck), dihydrogen hexachloroiridate(IV) hydrate ($H_2IrCl_6 \cdot xH_2O$, Sigma-Aldrich), Hydrochloric acid fuming (HCl, Merck, 37%), gamma alumina and alumina/silica (S_{BET}=187-200 m^2g^{-1}, Homemade products), and aluminosilicate (MCM-41, SiO_2 (97 wt%): Al_2O_3 (3 wt%), S_{BET}=920 m^2g^{-1}, Homemade product) were all used as received without further purification. Characterizations of the supports are summarized in Table 1.

The support materials were dried at 120°C for 12 h in the muffle oven flowing to remove moisture. One way of preparing supported iridium catalysts is the wetness aqueous impregnation method. First, an aqueous solution of $H_2IrCl_6 \cdot xH_2O$ precursor was prepared at room temperature and remained overnight. In this procedure, about 1 g of catalyst support (gamma-alumina and aluminosilicate) was impregnated with the solution of hexachloroiridic acid at the appropriate concentration to obtain the desired percentage of metal, and allowed to stand with occasional stirring at 60°C. In addition, HCl was added in the hexachloroiridate solution to decrease the pH. An oxide surface contains terminal hydroxyl groups that protonate or deprotonate depending of the acidity of the impregnating solution. Cations are absorbed at high pH on alumina, and anions are absorbed at low pH. The impregnation was followed by drying in air at 80°C for 12 h, and then calcined at 400°C for 3 h at a rate of 2°C/min. For high loaded iridium catalysts, the whole procedure was repeated three times to obtain the successive loading levels. Prior to the catalytic reaction, the catalysts were reduced with pure H_2 at 400°C for 2 h. The starting weight ratio iridium/support was maintained constant for all preparations and corresponds to iridium load (related to the mass of the carrier) of 20% (w/w). The final samples were denoted as Ir-XAlYSi, which are listed in Table 1.

Characterization of the catalyst samples

The specific surface area of the carriers and catalysts was evaluated by means of Brunauer–Emmett–Teller (BET) analysis. The N_2 adsorption–desorption isotherms were recorded on a BELSORP Mini, Microtrac Bel Corp. The catalysts were heated to remove physically bonded impurities from the surface at 150°C in inert gas for 5 h. TPR data were obtained in a flow system. The catalyst

was placed in a TPR reactor and pretreated in Ar at 300°C for 1 h. When the reactor was cooled to room temperature again, an H_2–Ar mixed gas was introduced. The temperature was raised at a constant rate, and the amount of H_2 uptake during the reduction was measured by a TCD. X-ray Diffraction (XRD) studies were carried out in a PANalytical X'Pert diffractometer equipped with a Cu Ka radiation. A field emission electron microscope coupled to an energy-dispersive spectrometer (FESEM-EDS) model MIRA3 Tescan, FEG was used to evaluate the morphology and the surface chemical composition of catalyst samples, both before and after the test campaigns. High resolution transmission electron microscopy (HRTEM) analysis was performed with an FEI Tecnai F20 microscope. Thermogravimetric analysis (TGA) was carried out using Linseys, STA 1600 apparatus. Thermal treatments were determined in a temperature range of 25-1000°C at the rate of 10°C min^{-1}. Catalysts resistance to mechanical compression was verified by placing spherical particles on a steel surface. The surface of granular was exposed to increasing pressures by a piston. Six runs were performed for each catalyst, and averaged.

Catalytic experiments

The self-designed system was applied for the decomposition of hydrazine monohydrate, with a sealed stainless steel reactor, a gas outlet, a safety valve, and an injector syringe. First, 0.1 g of granules was placed in the reactor. The decomposition was initiated by introducing 10 mL $N_2H_4 \cdot H_2O$ into the reactor. The N_2 and H_2 gaseous product was passed through a trap containing 1 M HCl to the absorption of ammonia, and volume of gases measured via an electronic balance by a gravimetric water-displacement method, and recorded by data acquisition software. The gas volume was used to calculate the number of gas moles from the molar ratio in Eq. (1):

$$\lambda = \frac{n(N_2) + n(H_2)}{n(N_2H_4)} \tag{1}$$

The selectivity of H_2 generation (X) was calculated following Eq. (2).

$$X = \frac{3\lambda - 1}{8} \left[\lambda = \frac{n(N_2) + n(H_2)}{n(N_2H_4)} \right] \tag{2}$$

The turnover frequency value (TOF) or the reaction rate (h^{-1}) was calculated in the 80% conversion of $N_2H_4 \cdot H_2O$ as follows:

$$TOF = \frac{PV}{3n_{metal}RTt} \tag{3}$$

where, P is the atmospheric pressure, V is the volume of generating gases (H_2 and N_2), R is the universal gas constant, T is the reaction temperature, n_{metal} is the mole number of iridium.

RESULTS AND DISCUSSION

Four different supporting materials were taken into account: alumina and alumina-silica with different molar ratios (97:3, 3:97, 50:50). The choice of the catalyst supports was driven by the aim of validating the effectiveness of the proposed iridium deposition method on supports with the same values of specific surface area and, at the same loading of the different carriers. Table 1 shows the physical properties of the supports used in the present study. Spheres with a diameter of 2 mm were used as catalyst supports.

Also, Table 1 presents H_2-TPR data of the iridium catalysts. For Ir-100Al catalyst, the hydrogen consumption peak was centered at 234°C, which represented the reduction of IrO$_2$ to metallic iridium. For Ir-97Al3Si catalyst, the main hydrogen consumption peak was one single peak around 354°C, much higher than that for Ir/γ-Al$_2$O$_3$ catalyst, indicating that the addition of SiO$_2$ significantly promoted reduction of Ir. The reason for this promotion was larger clusters of iridium. Therefore, this effect leads to the simultaneous reduction of Ir at higher temperatures. After calcination of Ir-3Al97Si at 400°C, hydrogen consumption maxima appeared at 227°C. TPR-H$_2$

Table 1. Main characteristics of catalyst carriers.

Catalyst ID	Material	γ-Al$_2$O$_3$ (wt%)	SiO$_2$ (wt%)	Diameter (mm)	H$_2$-TPR (°C)
Ir-100Al	Ir/γ-Al$_2$O$_3$	100	0	2	234
Ir-97Al3Si	Ir/Aluminosilicate	97	3	2	354
Ir-50Al50Si	Ir/γ-Al$_2$O$_3$/SiO$_2$	50	50	2	215, 331
Ir-3Al97Si	Ir/Aluminosilicate	3	97	2	227

Table 2. BET properties of iridium coated catalyst.

Composition	S_{BET} of support (m^2g^{-1})	S_{BET} (m^2g^{-1})	Pore volume (cm^3/g)	Pore Diameter (nm)	Mechanical resistance (MPa)
Ir-100Al	187	178	0.3	6	11.66
Ir-97Al3Si	198	74	0.1	8	4.11
Ir-50Al50Si	200	83	0.4	10	5.01
Ir-3Al97Si	920	413	0.7	7	0

profile of Ir-50Al50Si shows a small peak assigned to the reduction of iridium strongly bonded with the support surface at approximately 215°C and the peak in the range 331°C, which testify the presence of different IrO_x species. The metal–support interactions are indicated by the presence of larger clusters of iridium supported on Ir-97Al3Si and Ir-50Al50Si.

Surface area analysis

The BET surface area and pore volume before and after catalyst coating in four different
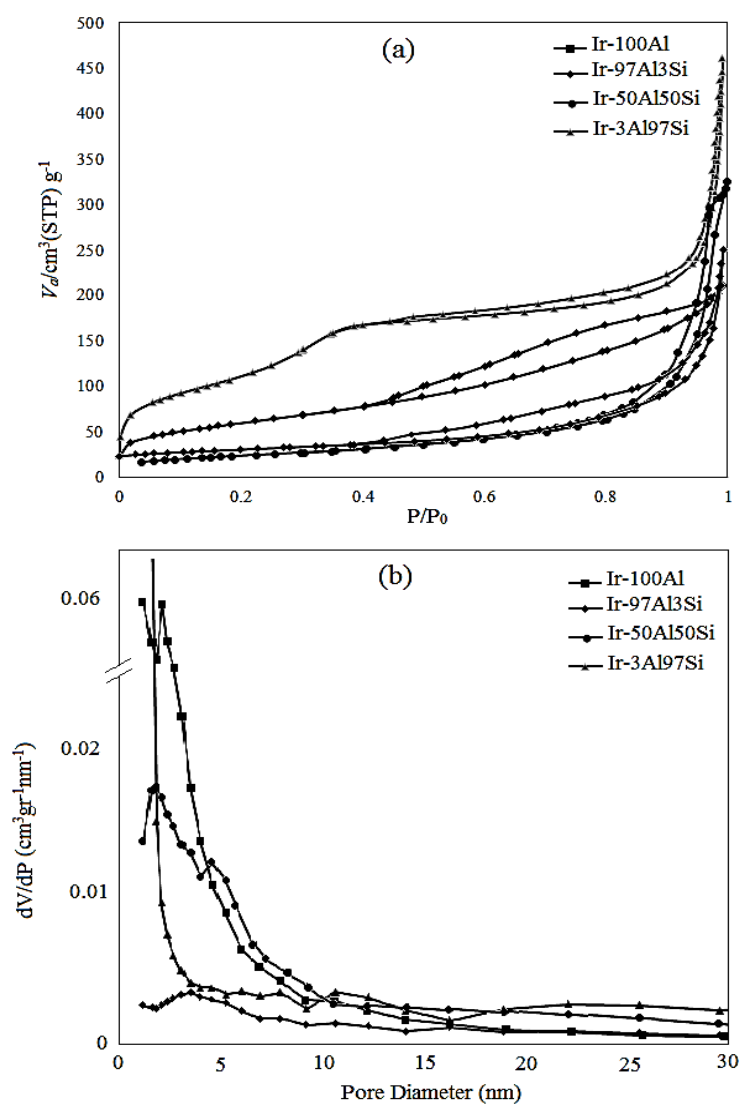

Fig. 1. (a) Nitrogen adsorption–desorption isotherms and (b) pore size distribution curves for the different catalysts.

supports are summarized in Table 2. The nitrogen adsorption–desorption isotherms of mesoporous alumina and aluminosilicate supports with the same loading amounts all yield type IV curves with H1-shaped hysteresis loops (Fig. 1a), suggesting their uniform cylindrical pores. It exhibits a Brunauer-Emmett-Teller surface area of 187 m^2/g for 100Al, 198 m^2/g for 97Al3Si, and 200 m^2/g for 50Al50Si. But, the support made from 97 wt% silica will have a total surface area of approximately 920 m^2/g. On a weight basis, the addition of Ir reduces the total surface area, measured by N$_2$ adsorption. Such behaviour can be explained by considering the blockage of support pores with iridium nanoparticles during impregnation [29]. Barrett-Joyner-Halenda (BJH) calculations derived from the desorption branches reveal a narrow pore size distribution centered at 6-12 nm, (Fig. 1b).

The large surface areas, and narrow pore size distributions combined with well-dispersed iridium nanoparticles enhance the hydrazine decomposition of these ordered mesoporous gamma-alumina. Also, mechanical resistances of the aluminosilicate supports are less when compared to gamma-alumina support (Table 2). An increasing amount of porosity decreases the mechanical resistance of the catalyst, while the sufficient strength of the support is subjected to extremely rough conditions [25, 26]. The lower mechanical resistance of the aluminosilicate supports (compared to alumina support) is attributed to the type of interaction and porosity.

Thermal gravimetric analysis

The TGA curves of the catalysts in the air atmosphere reveals that the total weight losses given are: 8.48 wt % (Ir-100Al), 0.5 wt% (Ir-97Al3Si), 4.2 wt % (Ir-3Al97Si), and 8.31 wt % (Ir-50Al50Si), see Fig. 2. However, the TGA curves for total samples showed the same trend of decrease mass loss as the temperature approached 1000°C. In each catalyst, the weight loss occurs from room temperature to about 300°C. In this range, the evaporation of the solvents and the burning of residual organic molecules usually occur. The evaporation of water in open pores in the samples and the combustion and decomposition of the organic compounds are continued. Since the catalyst was calcined at 400°C, the peaks above this temperature are partly due to the dehydroxylation of the support OH groups.[32] Then a small increase in mass of about 400–600°C occurs, that can be assigned to slowly oxidizing iridium metal, followed by a rapid mass loss [33]. However, the weight changes of all catalysts are generally low at this temperature range.
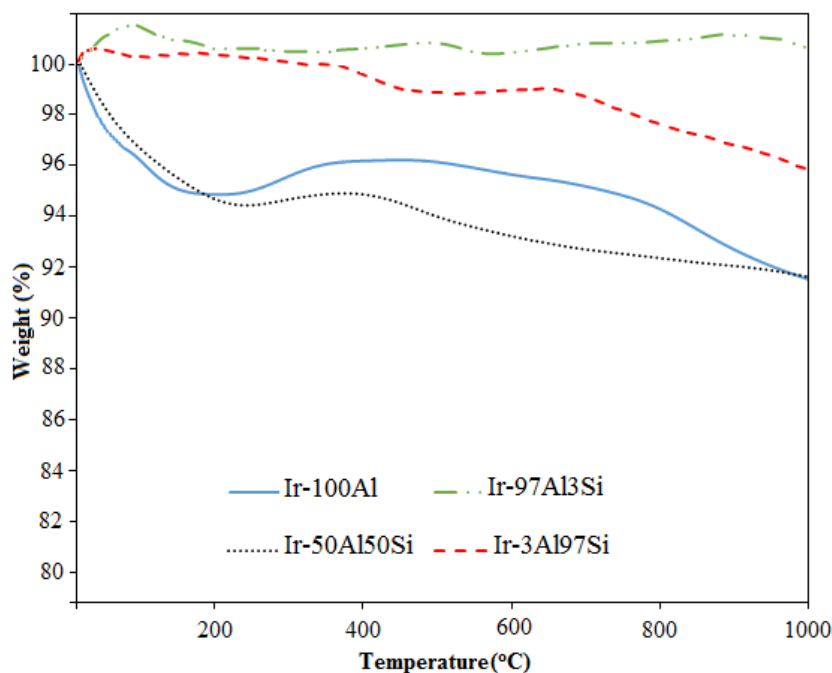

Fig. 2. TGA thermograms of catalysts.

X-Ray diffraction analysis

The identification of the crystallizing phases has been assessed by X-ray diffraction analysis. The analysis of the XRD profiles allows the acquisition of information about the mean size of the crystallites. Fig. 3 shows the patterns of the Ir catalyst as function of support compositions. The XRD patterns showed three major peaks at ~40.5°, 47° and 69°, which correspond to three crystal faces of iridium: (1 1 1), (2 0 0), and (2 2 0), respectively, according to the XRD standard card (JCPDS Card No. 06–0598). These peak positions were assigned to Ir metal phase in Ir-100Al, Ir-97Al3Si, and Ir-3Al97Si. The sharper diffraction peak at 2θ=40.5° corresponds to the Ir (1 1 1) plane [34]. XRD profile of Ir-50Al50Si catalyst showed the peaks of IrO_2 with a JCPDS (No. 15-870) standard pattern. No diffraction peak was observed for iridium metal in the XRD profile of Ir-50Al50Si catalyst. In the XRD pattern of Ir-50Al50Si, the prominent peaks of IrO_2 appeared at 2θ ~27°, 34°, and 53°, and this pattern was also obtained with the significant peaks at 2θ ~45° and 65° which were indexed as γ-Al_2O_3. Reflections of Ir-50Al50Si catalyst are indexed as (1 1 0), (1 0 1), (2 0 0) and (2 1 1). The sharper

diffraction peak centered at 2θ=34° in the XRD spectrum can be attributed to the structure (1 0 1) of IrO_2 [35]. The spectra clearly indicate the oxidation of iridium to iridium oxide in Ir-50Al50Si catalyst after reduction in hydrogen, because of physical mixture of the components. It was noted that adding the silica in alumina resulted in a decrease in the average crystallite size, except for Ir-50Al50Si. The mean iridium particle sizes were determined from the line broadening of the diffraction lines, using the Scherrer equation, which ranged from 19 nm (Ir-100Al), 16 nm (Ir-97Al3Si), 16 nm (Ir-3Al97Si) to 28 nm (Ir-50Al50Si). Notably, the aluminosilicate support perturbs the crystal growth of Ir nanocrystallites, which would affect the catalytic activity. It seemed that smaller particle size was not favorable for obtaining high activity in decomposition of hydrazine hydrate. Hence, the metal particle size of supported iridium catalysts is an important factor affecting catalytic behavior.

High-resolution transmission electron microscopy

The HRTEM images in Fig. 4 clearly showed the dispersion of iridium nanoparticles with
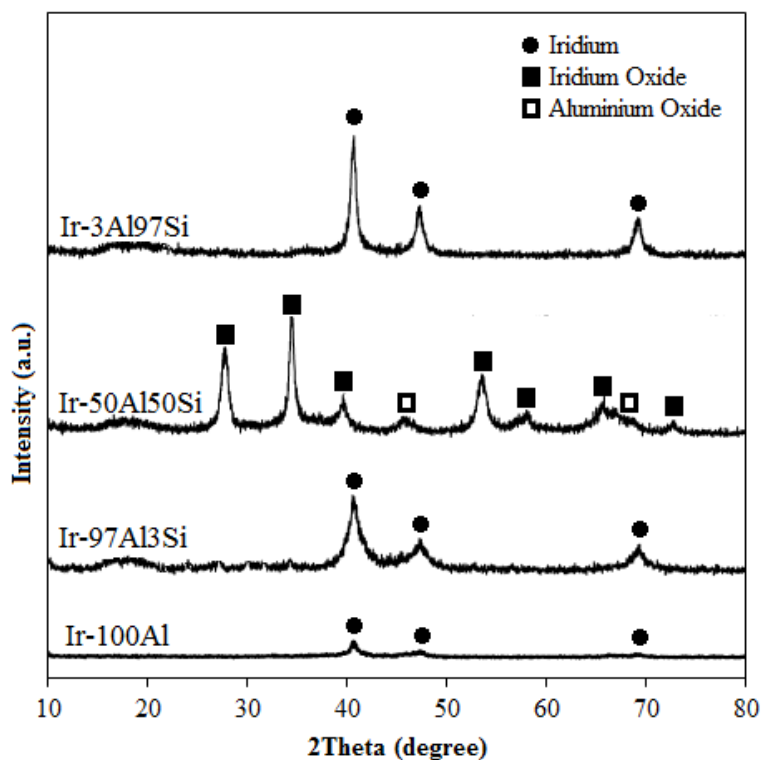

Fig. 3. XRD patterns of the iridium catalyst on different supports before decomposition of hydrous hydrazine.
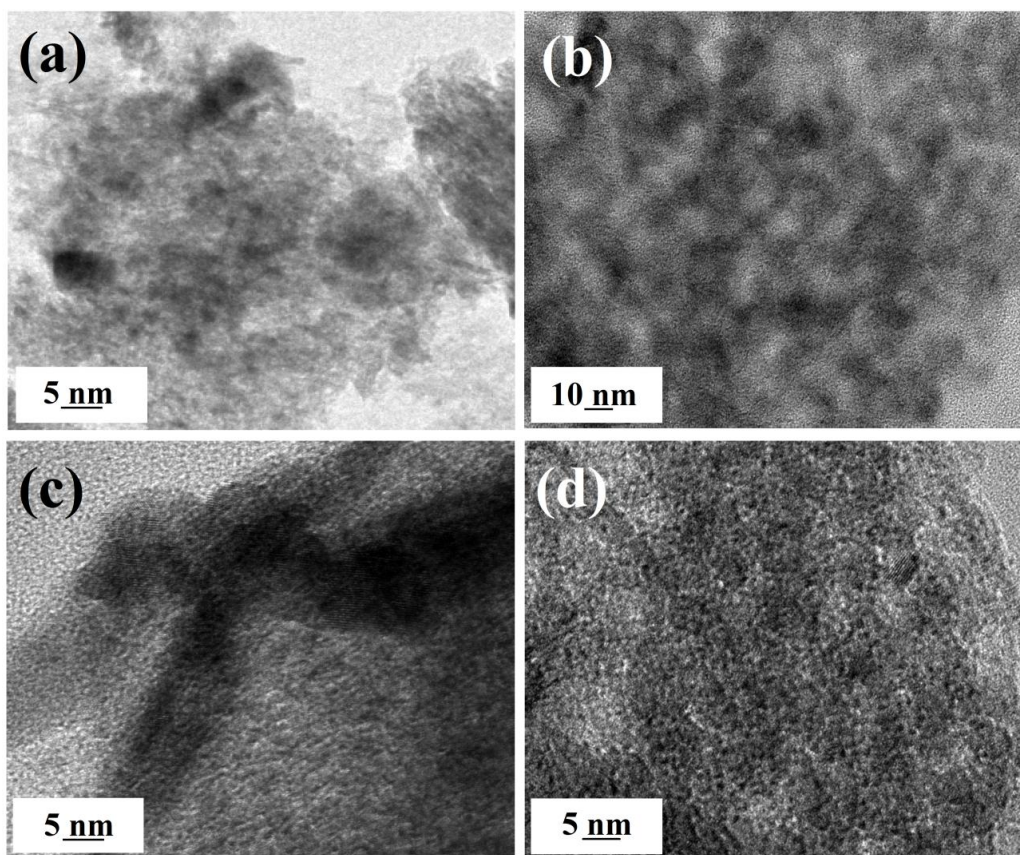
Fig. 4. HRTEM micrographs of (a) Ir-100Al, (b) Ir-97Al3Si, (c) Ir-50Al50Si, and (d) Ir-3Al97Si.

an average size of around 15-20 nm, which is in accordance with the XRD result. It is found a good agreement between the results from XRD analysis and TEM analysis and hence, the results from TEM analysis are shown the smaller particle size of Ir-97Al3Si and Ir-3Al97Si catalysts (~15-16 nm), and Ir-100Al catalyst has bigger particle size (~20 nm) than both these catalysts. The particle shape seemed to be spherical, but also smaller size of iridium crystallite exists on Ir/Aluminosilicate than on Ir/γ-Al$_2$O$_3$. There exists a strong interaction between iridium and γ-Al$_2$O$_3$ in Ir-100Al, which leads to a better anchoring of iridium on γ-Al$_2$O$_3$ than on SiO$_2$. Thus, γ-Al$_2$O$_3$ seems to be a good support for dispersing iridium with high loading [36]. Most notably the dispersion of the active phase decreased in aluminosilicate compared to alumina. These changes could be connected with the observed data in catalyst activity.

Scanning electron microscopy analysis

The surfaces of the prepared samples were investigated by FESEM. Fig. 5a presents the spherical morphology of iridium on γ-Al$_2$O$_3$ granules. For Ir-97Al3Si, Ir-3Al97Si, and Ir-50Al50Si catalysts, metal particles were observed of different shapes and sizes and were not uniformly distributed on the alumina surface (Fig. 5b, c and d). In contrast to the aluminosilicate catalyst (Fig. 5c and d), Ir-100Al show the homogenous dispersion of iridium nanoparticles over the surface of γ-Al$_2$O$_3$ support due to the strong interaction iridium and alumina, which was later manifested by hydrazine catalysis over this optimal catalyst. Here, high metal dispersion of nanoparticles in alumina surface corresponded to the better catalytic activity of iridium particles [37].

Catalytic activity evaluation

The catalytic properties of Ir/γ-Al$_2$O$_3$ catalyst for the decomposition reactions of N$_2$H$_4$·H$_2$O were examined and compared with the corresponding Ir/aluminosilicate catalysts. It has been reported that the catalytic performance was quite
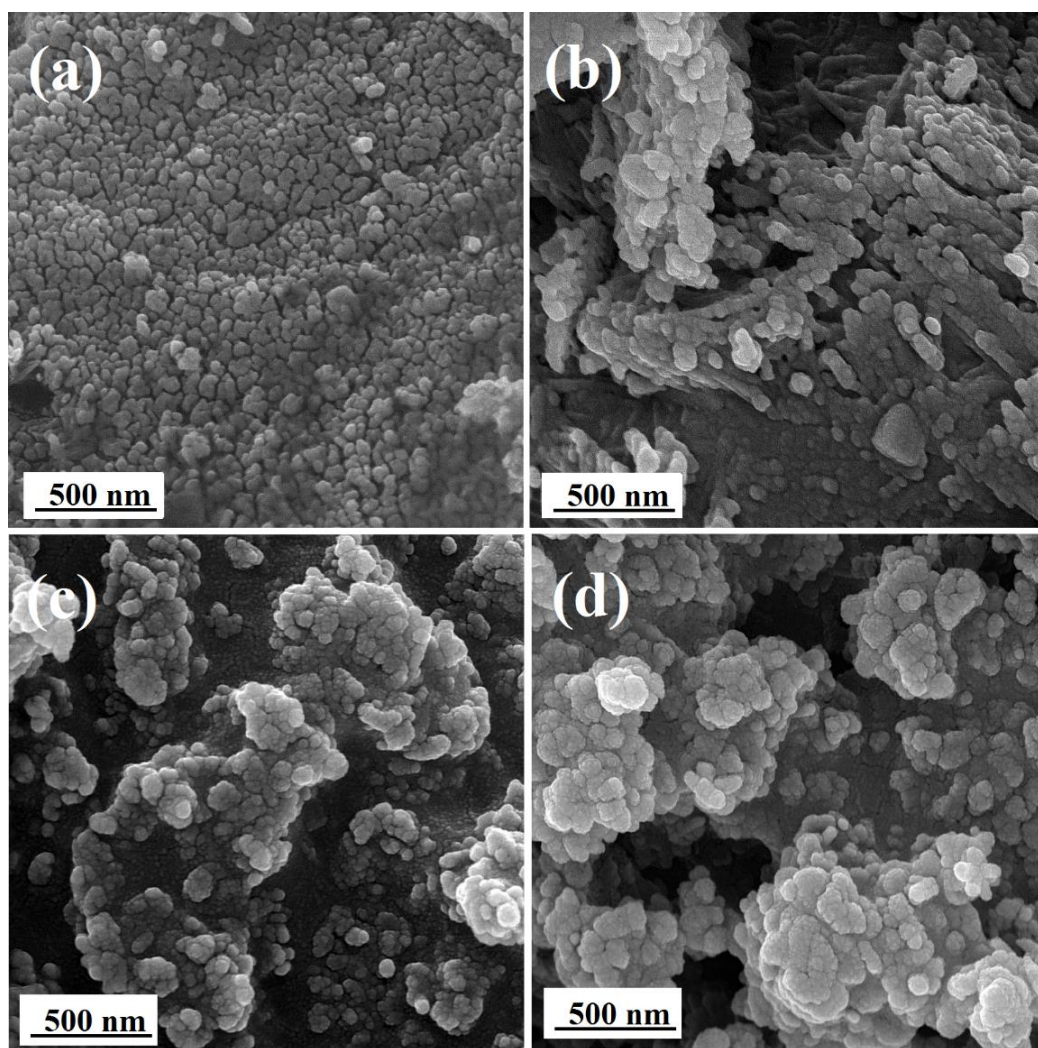
Fig. 5. FESEM micrographs of (a) Ir-100Al, (b) Ir-97Al3Si, (c) Ir-50Al50Si, and (d) Ir-3Al97Si.

sensitive to the carriers [31–33]. N_2H_4 molecules can be adsorbed on Ir surface accompanied with decomposition through intramolecular or intermolecular reaction. Hydrazine bonds via both N atoms with the N-N axis paralleling to the iridium surface. N-N bond cleavage will facilitate ammonia formation.

Hydrazine molecules through exothermic reactions decompose into NH_3, H_2, and N_2 on the iridium catalyst. NH_3 and N_2 are the main gas products at low temperatures, and the H_2 selectivity is low [41]. Ammonia is not only a product but also an intermediate. Iridium nanoparticle is an active center for intermediate ammonia decomposition. The reaction can be described in two steps [42]:

$$3N_2H_4 \rightarrow 4NH_3 + N_2 \ (Exothermic) \tag{4}$$

$$4NH_3 \rightarrow 2N_2 + 6H_2 \ (Endothermic) \tag{5}$$

Decomposition of ammonia is endothermic, and the temperature decreased after this decomposition [43]. Thereby, it is a great challenge of developing efficient catalysts for the selective decomposition of hydrazine to H_2 production. The NH_3 dissociation should be adjusted, since the working point moves away from the optimum at high dissociation, thus affecting system performance. Once the reaction is catalyzed, hydrazine starts decomposing, and

inevitably, is accompanied by increasing ammonia, which is along with ammonia decomposition. The decomposition of NH_3 is slow due to the high activation temperature of this reaction. Hence, when mass fraction of ammonia starts decreasing, decomposition is more important. Hydrogen and nitrogen gases will increase with hydrazine and ammonia decomposition, and this high pressure of hydrogen causes to inhibit the rate of ammonia decomposition [44]. Iridium active phase supported on four different supports –alumina and aluminosilicate- had the ability to convert hydrazine completely into products at 25°C. With increasing silica content, the activity decreased. As the active phase and its composition are the same for all studied catalysts, the variations are due to the action of the support such as effect on dispersion of the active phase. As shown in Fig. 6a, Ir-50Al50Si catalyst was very inactive, and other Ir/ aluminosilicate catalyst (Ir-97Al3Si and Ir-3Al97Si)
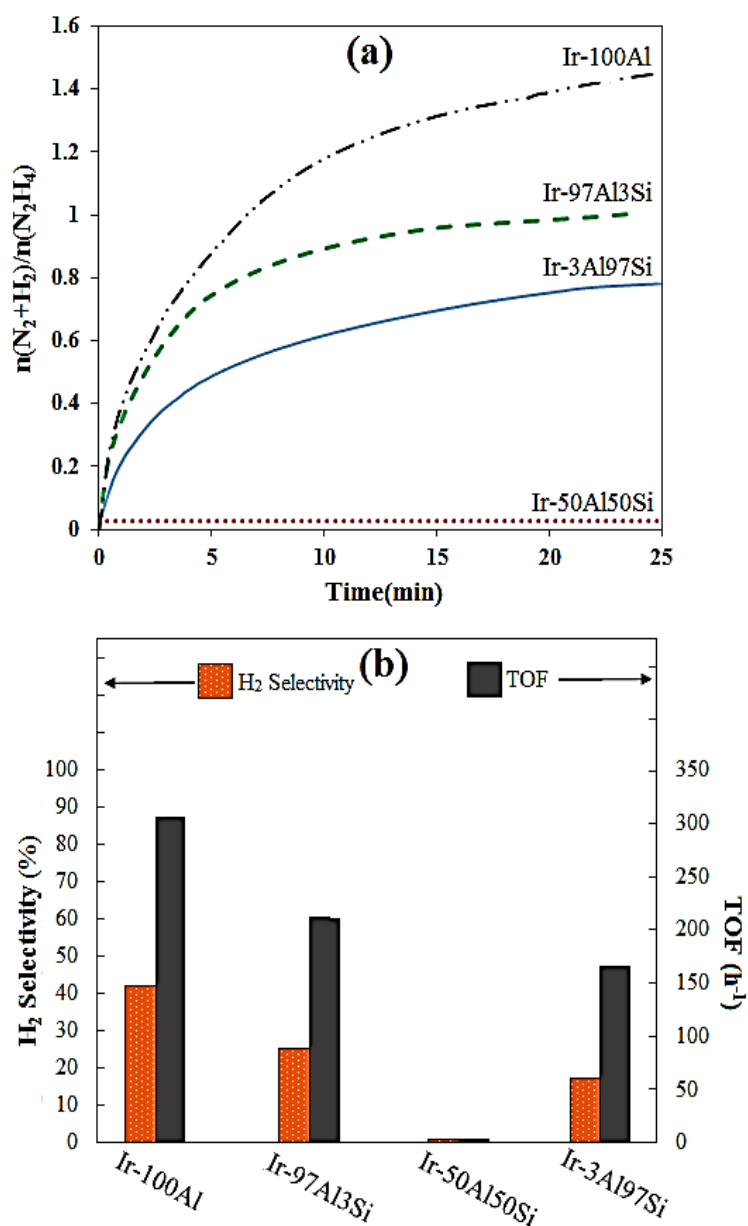

Fig. 6. (a) Time profiles, and (b) the comparison of selectivity and reaction rate for hydrous hydrazine decomposition of iridium catalysts.

exhibited low catalytic activity, and moderate H_2 selectivity in catalytic decomposition of $N_2H_4 \cdot H_2O$. However, Ir/γ-Al$_2$O$_3$, the resulting showed drastically enhanced catalytic performance. The γ-Al$_2$O$_3$-supported iridium catalyst affording mostly decomposition products, it can be inferred to be have higher dispersion due to stronger iridium-alumina interaction. These findings emphasise the interaction between iridium atoms, and also iridium and Al$_2$O$_3$ on the high-loading Ir/γ-Al$_2$O$_3$ catalysts [36]. Hydrazine molecules can be adsorbed on iridium nanoparticles in different conformations, then decomposition occurs through intramolecular or intermolecular reaction, depending upon the nature and structure of metal catalysts [45]. Specifically, N_2H_4 bonds to the surface via both N atoms with the N-N axis paralleling to the surface (cis conformation), rendering the N-N bond more perturbed and more favorable to be cleaved. N-N bond cleavage will facilitate NH_3 formation (low H_2 selectivity) via a lower-energy intermolecular reaction path [46].

Interestingly, NH_3 conversions on aluminosilicate catalysts are much lower than those on alumina counterparts.

Fig. 6b plots the hydrogen selectivity and the turnover frequency (TOF) of catalysts versus the support types. It can be seen these that the TOF of the iridium catalysts dropped with the increase in silica content of support. This plays an important role on release of gas product. The H_2 selectivity over Ir/γ-Al$_2$O$_3$ catalysts was decreased from 42% to over 25% and 17% after addition of 3 and 97 wt% SiO$_2$ into the support (Ir-97Al3Si and Ir-3Al97Si), respectively. Ir-50Al50Si catalyst did not exhibit any activity in hydrous hydrazine decomposition. Thus, the activity of Ir toward hydrazine decomposition was greatly changed by support, which was beneficial for H_2 selectivity. The rate of catalytic reaction per unit mole of iridium for the Ir-100Al catalyst is ~306 h^{-1}, which stands out as the top level of this $N_2H_4 \cdot H_2O$ decomposition catalysts. The H_2 selectivity was 42% over Ir-100Al, which is surprisingly high because
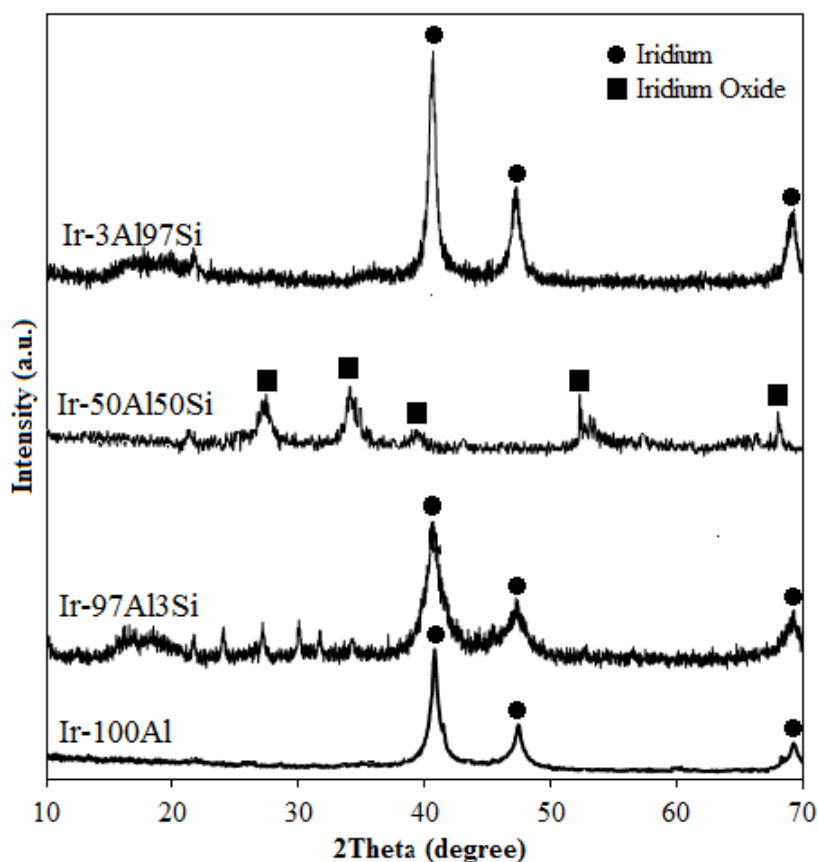

Fig. 7. XRD patterns of the iridium catalyst on different supports after decomposition of hydrous hydrazine.

Ir nanoparticle itself exhibited high activity for hydrazine decomposition to produce NH_3 instead of H_2. This implies that γ-Al_2O_3 exhibits certain ammonia decomposition activity. These results imply that iridium sites are also an active center for intermediate NH_3 decomposition in hydrazine decomposition reaction. Interestingly, the NH_3 conversion on Ir/γ-Al_2O_3 catalyst is much higher than those of Ir/Aluminosilicate counterparts, and iridium nanoparticles are dispersed more homogeneous on the surface of γ-Al_2O_3. Thus, it is obvious that higher NH_3 conversion on Ir/γ-Al_2O_3 catalyst, this could be attributed to highly dispersed iridium active sites. The results shown in Fig. 6b clearly show that the operation of catalyst is strongly dependent on the nature of the support. The interaction between reactant and catalyst play an important role in chemical reactions, especially the bond cleavage reaction [46]. According to the bond order conservation theory, weaker intramolecular bonding causes stronger adsorption, thus leading the catalyst higher activity towards a dissociative reaction. The data obtained indicate the suitability of γ-Al_2O_3, as compared to aluminosilicate as supports. In this context, one issue that has attracted attention in the literature is whether or not the carrier type influences the catalytic activity or it is just a way of achieving different iridium dispersion, to address specifically this point.

The XRD patterns for the iridium catalysts after decomposition of hydrazine monohydrate are shown in Fig. 7. Three catalysts (Ir-100Al, Ir-97Al3Si, and Ir-3Al97Si) exhibit the main reflection lines of iridium nanoparticles (2θ = 40.5°, 47° and 69°). This suggests that after hydrazine decomposition, iridium nanoparticles are active in the three catalysts without becoming oxidized. As observed for the catalysts before hydrazine monohydrate decomposition, the main lines characteristic of IrO_2 (2θ = 27°, 34°, and 53°) were detected for the Ir-50Al50Si catalyst. IrO_2 particles in the Ir-50Al50Si catalyst remain in the same oxidized phase, although they did not participate in the decomposition reaction. These phase

stabilities are essential for the long lifetime of the iridium catalysts. Also, stable particle on surface is important during the decomposition reaction that the FESEM analysis used to detect it. The FESEM images of the catalyst surfaces before and after hydrazine decomposition are quite different (Fig. 8). It is noted that before and after decomposition of hydrazine in Fig. 7a, the surface character of 100Al remained almost the same. This result strongly indicates that the type of support iridium catalyst does not blocked and the interaction between iridium and support is suitable; the results agree with BET surface area in Table 3. Significant growth of the particles on catalyst surface with Ir-50Al50Si was similar before and after being used in reactor, indicating that the sintering of iridium particles may be the deactivation reason of this catalyst, as shown in Fig. 7c. For the Ir-97Al3Si and Ir-3Al97Si catalysts (Table 3), the surface area was increased after decomposition of hydrous hydrazine, indicating that the addition of SiO_2 significantly promoted sintering of Ir and poor interaction. There is the possibility that the release of confinement of nanoparticles inside the pore channels of the catalyst resulting an increase in the BET surface area. This growth are also shown in the FESEM images (Fig. 8b and d). The Ir-97Al3Si have surface areas of 63 m^2/g after decomposition of hydrous hydrazine, compared with 74 m^2/g before decomposition of hydrous hydrazine. Similarly, the Ir-3Al97Si has a surface area of 391 m^2/g after test, compared with 413 m^2/g before test. However, we may suggest that the different interaction occurring between iridium and support is probably related to the variation of the surface structures resulting from different silica content in alumina.

CONCLUSIONS

Four different supports (alumina and aluminosilicate) were used for preparation of iridium catalysts to be used in the hydrazine monohydrate decomposition. A reasonable explanation to justify the large differences in activity between the catalysts prepared following

Table 3. BET properties of iridium coated catalyst before and after decomposition of hydrous hydrazine.

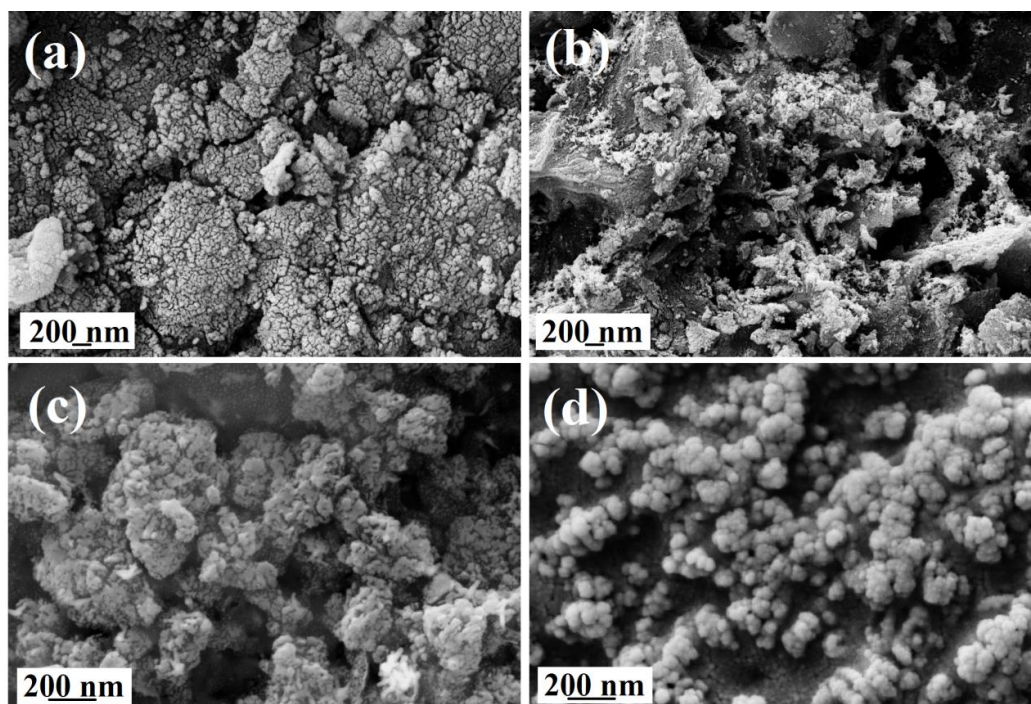| Composition	S_{BET} (m^2g^{-1})	
	Before test	After test
Ir-100Al	178	176
Ir-97Al3Si	74	63
Ir-50Al50Si	83	82
Ir-3Al97Si	413	391

Fig. 8. FESEM micrographs of (a) Ir-100Al, (b) Ir-97Al3Si, (c) Ir-50Al50Si, and (d) Ir-3Al97Si, after decomposition of hydrous hydrazine.

the same method, but different silica content in the support relies on accepting that the free surface of iridium nanoparticles plays a role in catalysis. Most notably the dispersion of the active phase decreased in the following order Ir-50Al50Si >Ir-3Al97Si > Ir-97Al3Si > Ir-100Al. Moreover, the different active phase cluster size, acidic sites and support nature were reflected in differences inactive phase reducibility and in the character of iridium species. The aluminosilicate [SiO_2 (97 wt%): Al_2O_3 (3 wt%)]-supported Ir catalyst exhibited smaller extent of decomposition reaction and a larger extent of ammonia. As a result, ammonia was the main product, and less gas products were yielded in comparison with the other two catalysts. On the other hand, the Al_2O_3-supported Ir catalyst exhibited increased selectivity to hydrogen, plausible due to the better active phase distribution. The results provide clear evidence that the most active catalysts for the hydrazine decomposition are those that contain the lowest silica percentage on the alumina support.

CONFLICT OF INTERESTS

The authors declare that there is no conflict of interests regarding the publication of this paper.

REFERENCES

1. Razavi FS, Morassaei MS, Salehabadi A, Ghiyasiyan-Arani M, Salavati-Niasari M. Structural characterization and electrochemical hydrogen sorption performances of the polycrystalline $Ba_2Co_9O_{14}$ nanostructures. J Alloys Compd. 2019;777:252-258.
2. Khorasanizadeh MH, Ghiyasiyan-Arani M, Monsef R, Salavati-Niasari M, Moayedi H. Ultrasound-accelerated synthesis of uniform $DyVO_4$ nanoparticles as high activity visible-light-driven photocatalyst. Ultrason Sonochem. 2019;59:104719.
3. Monsef R, Ghiyasiyan-Arani M, Salavati-Niasari M. Utilizing of neodymium vanadate nanoparticles as an efficient catalyst to boost the photocatalytic water purification. J Environ Manage. 2019;230:266-281.
4. Ghiyasiyan-Arani M, Salavati-Niasari M. Effect of $Li_2CoMn_3O_8$ Nanostructures Synthesized by a Combustion Method on Montmorillonite K10 as a Potential Hydrogen Storage Material. The Journal of Physical Chemistry C. 2018;122(29):16498-16509.
5. Sun J, Zheng M, Wang X, Wang A, Cheng R, Li T, et al. Catalytic Performance of Activated Carbon Supported Tungsten Carbide for Hydrazine Decomposition. Catal Lett. 2008;123(1-2):150-155.
6. Vieira R, Pham-Huu C, Keller N, Ledoux MJ. New carbon nanofiber/graphite felt composite for use as a catalyst support for hydrazine catalytic decomposition. Chem Commun. 2002(9):954-955.
7. Manukyan KV, Cross A, Rouvimov S, Miller J, Mukasyan AS, Wolf EE. Low temperature decomposition of hydrous hydrazine over FeNi/Cu nanoparticles. Applied Catalysis A:

General. 2014;476:47-53.

8. Satterfield CN. ChemInform Abstract: INDUSTRIAL HETEROGENEOUS CATALYSIS: AN OVERVIEW. Chemischer Informationsdienst. 1982;13(9).

9. Trueba M, Trasatti SP. γ-Alumina as a Support for Catalysts: A Review of Fundamental Aspects. Eur J Inorg Chem. 2005;2005(17):3393-3403.

10. Héroguel F, Siddiqi G, Detwiler MD, Zemlyanov DY, Safonova OV, Copéret C. Simultaneous generation of mild acidic functionalities and small supported Ir NPs from alumina-supported well-defined iridium siloxide. J Catal. 2015;321:81-89.

11. Janjua NK, Firdous N, Bhatti AS, Khan ZS. Preparation and catalytic evaluation of Ir and Ru catalysts supported in γ-Al_2O_3 for hydrazine decomposition in a 1N microthruster. Applied Catalysis A: General. 2014;479:9-16.

12. Amirsardari Z, Aghdam RM, Salavati-Niasari M, Shakhesi S. Facile Carbothermal Reduction Synthesis of ZrB_2 Nanoparticles: The Effect of Starting Precursors. Mater Manuf Processes. 2015;31(2):134-140.

13. Amirsardari Z, Aghdam RM, Salavati-Niasari M, Shakhesi S. Preparation and characterization of a novel hetero-nanostructure of zirconium diboride nanoparticle-coated multi-walled carbon nanotubes. RSC Adv. 2014;4(106):61409-61414.

14. Amirsardari Z, Aghdam RM, Salavati-Niasari M, Jahannama MR. The Effect of Starting Precursors on Size and Shape Modification of ZrB_2 Ceramic Nanoparticles. Journal of Nanoscience and Nanotechnology. 2015;15(12):10017-10021.

15. Amirsardari Z, Aghdam RM, Jahannama MR. Role of surface thermal properties of HfB_2 nanoparticles on heat flow in MWCNT/novolac composites. Bull Mater Sci. 2018;41(1).

16. Samain L, Jaworski A, Edén M, Ladd DM, Seo D-K, Javier Garcia-Garcia F, et al. Structural analysis of highly porous γ-Al_2O_3. J Solid State Chem. 2014;217:1-8.

17. Phung TK, Herrera C, Larrubia MÁ, García-Diéguez M, Finocchio E, Alemany LJ, et al. Surface and catalytic properties of some γ-Al_2O_3 powders. Applied Catalysis A: General. 2014;483:41-51.

18. Petty WL. Variation in Shell 405 Catalyst Physical Characteristics, Test Catalyst Preparation. Defense Technical Information Center; 1973 1973/07/01.

19. Rajagopal S, Marzari JA, Miranda R. Silica-Alumina-Supported Mo Oxide Catalysts: Genesis and Demise of Brønsted-Lewis Acidity. J Catal. 1995;151(1):192-203.

20. Tong DG, Zeng XL, Chu W, Wang D, Wu P. Preparation of monodispersed cobalt–boron spherical nanoparticles and their behavior during the catalytic decomposition of hydrous hydrazine. Mater Res Bull. 2010;45(4):442-447.

21. Fan C, Wu T, Kaden WE, Anderson SL. Cluster size effects on hydrazine decomposition on Irn/Al_2O_3/NiAl(110). Surf Sci. 2006;600(2):461-467.

22. Zheng M, Chen X, Cheng R, Li N, Sun J, Wang X, et al. Catalytic decomposition of hydrazine on iron nitride catalysts. Catal Commun. 2006;7(3):187-191.

23. Singh SK, Iizuka Y, Xu Q. Nickel-palladium nanoparticle catalyzed hydrogen generation from hydrous hydrazine for chemical hydrogen storage. Int J Hydrogen Energy. 2011;36(18):11794-11801.

24. Singh SK, Xu Q. Nanocatalysts for hydrogen generation from hydrazine. Catalysis Science & Technology. 2013;3(8):1889.

25. Cao C, Li Z, Li Y, Wang G, Yuan S, Li H, et al. Synthesis, characterization and electrochemical applications of Ir@ SiO_2 composite microspheres. Colloids Surf Physicochem Eng Aspects. 2017;529:979-984.

26. Amirsardari Z, Dourani A, Amirifar MA, Massoom NG, Jahannama MR. Controlled attachment of ultrafine iridium nanoparticles on mesoporous aluminosilicate granules with carbon nanotubes and acetyl acetone. Mater Chem Phys. 2020;239:122015.

27. Pekarik V, Peskova M, Guran R, Novacek J, Heger Z, Tripsianes K, et al. Visualization of stable ferritin complexes with palladium, rhodium and iridium nanoparticles detected by their catalytic activity in native polyacrylamide gels. Dalton Trans. 2017;46(40):13690-13694.

28. McVicker GB, Ziemiak JJ. ChemInform Abstract: Chemisorption properties of platinum and iridium supported on titania-alumina mixed-oxide carriers: evidence for strong metal-support interaction formation. Chemischer Informationsdienst. 1985;16(51).

29. Meille S, Lombardi M, Chevalier J, Montanaro L. Mechanical properties of porous ceramics in compression: On the transition between elastic, brittle, and cellular behavior. J Eur Ceram Soc. 2012;32(15):3959-3967.

30. Soares Neto TG, Cobo AJG, Cruz GM. Evolution of morphologic properties on the preparation of Ir/Al2O3 catalysts with high metallic contents. Appl Surf Sci. 2005;240(1-4):355-365.

31. Vuori H, Silvennoinen RJ, Lindblad M, Österholm H, Krause AOI. Beta Zeolite-Supported Iridium Catalysts by Gas Phase Deposition. Catal Lett. 2009;131(1-2):7-15.

32. Bayer G, Wiedemann HG. Formation, dissociation and expansion behavior of platinum group metal oxides (PdO, RuO_2, IrO_2). Thermochim Acta. 1975;11(1):79-88.

33. Moraes R, Thomas K, Thomas S, Van Donk S, Grasso G, Gilson J-P, et al. Ring opening of decalin and methylcyclohexane over bifunctional Ir/WO_3/Al_2O_3 catalysts. J Catal. 2013;299:30-43.

34. Chen R-S, Huang Y-S, Liang Y-M, Tsai D-S, Chi Y, Kai J-J. Growth control and characterization of vertically aligned IrO_2 nanorods. J Mater Chem. 2003;13(10):2525.

35. Li L, Wang X, Zhao X, Zheng M, Cheng R, Zhou L, et al. Microcalorimetric studies of the iridium catalyst for hydrazine decomposition reaction. Thermochim Acta. 2005;434(1-2):119-124.

36. Zhang J, Wang H, Dalai AK. Effects of metal content on activity and stability of Ni-Co bimetallic catalysts for CO_2 reforming of CH_4. Applied Catalysis A: General. 2008;339(2):121-129.

37. Singhania A, Krishnan VV, Bhaskarwar AN, Bhargava B, Parvatalu D, Banerjee S. Catalytic performance of bimetallic Ni-Pt nanoparticles supported on activated carbon, gamma-alumina, zirconia, and ceria for hydrogen production in sulfur-iodine thermochemical cycle. Int J Hydrogen Energy. 2016;41(25):10538-10546.

38. Gao X, Du C, Zhang C, Chen W. Copper Nanoclusters on Carbon Supports for the Electrochemical Oxidation and Detection of Hydrazine. ChemElectroChem. 2016;3(8):1266-1272.

39. Toyir J, Ramírez de la Piscina P, Fierro JLG, Homs Ns. Catalytic performance for CO_2 conversion to methanol of gallium-promoted copper-based catalysts: influence of metallic precursors. Applied Catalysis B: Environmental. 2001;34(4):255-266.

40. Singh SK, Zhang X-B, Xu Q. Room-Temperature Hydrogen

Generation from Hydrous Hydrazine for Chemical Hydrogen Storage. J Am Chem Soc. 2009;131(29):9894-9895.

41. Hwang CH, Lee SN, Baek SW, Han CY, Kim SK, Yu MJ. Effects of Catalyst Bed Failure on Thermochemical Phenomena for a Hydrazine Monopropellant Thruster Using Ir/Al$_2$O$_3$ Catalysts. Ind Eng Chem Res. 2012;51(15):5382-5393.

42. Chen X, Zhang T, Ying P, Zheng M, Wu W, Xia L, et al. A novel catalyst for hydrazine decomposition: molybdenum carbide supported on γ-Al$_2$O$_3$. Chem Commun. 2002(3):288-289.

43. Shankar V, Ram KA, Bhaskaran KA. Prediction of the concentration of hydrazine decomposition products along a granular catalytic bed. Acta Astronaut. 1984;11(6):287-299.

44. Holewinski A, Xin H, Nikolla E, Linic S. Identifying optimal active sites for heterogeneous catalysis by metal alloys based on molecular descriptors and electronic structure engineering. Current Opinion in Chemical Engineering. 2013;2(3):312-319.

45. Aika K. Hydrogenolysis of hydrazine over metals. J Catal. 1970;19(2):140-143.

46. Song S, Liu X, Li J, Pan J, Wang F, Xing Y, et al. Confining the Nucleation of Pt to In Situ Form (Pt-Enriched Cage)@CeO$_2$ Core@Shell Nanostructure as Excellent Catalysts for Hydrogenation Reactions. Adv Mater. 2017;29(28):1700495.